Available online at www.sciencedirect.com
SCIENCE DIRECT®
Journal of Solid State Chemistry 178 (2005) 2368–2375
JOURNAL OF SOLID STATE CHEMISTRY
www.elsevier.com/locate/jssc

Synthesis of MnOOH nanorods by cluster growth route from $[Mn_{12}O_{12}(RCOO)_{16}(H_2O)_n]$ ($R = CH_3$, C_2H_5). Rational conversion of MnOOH into Mn_3O_4 or MnO_2 Nanorods

Benjamin Folch[a], Joulia Larionova[a,*], Yannick Guari[a,*], Christian Guérin[a], Corine Reibel[b]

[a]*Laboratoire de Chimie Moléculaire et Organisation du Solide (LCMOS), UMR UMII-CNRS 5637, Université Montpellier II, Place E. Bataillon, 34095 Montpellier cedex 5, France*

[b]*Laboratoire de Physico-Chimie de la Matière Condensée (LPMC), UMR UMII-CNRS 5617, Université Montpellier II, Place E. Bataillon, 34095 Montpellier cedex 5, France*

Received 4 February 2005; received in revised form 19 May 2005; accepted 20 May 2005

Abstract

Single-crystalline nanorods of γ-MnOOH (manganite) phase with diameters of 120 nm and lengths of 1100 nm have been prepared using a new cluster growth route under low-temperature hydrothermal conditions starting from $[Mn_{12}O_{12}(CH_3COO)_{16}(H_2O)_4]\cdot 2CH_3COOH\cdot 4H_2O$ or $[Mn_{12}O_{12}(C_2H_5COO)_{16}(H_2O)_3]\cdot 4H_2O$ without any catalyst or template agents. The so-obtained nanorods were studied by X-ray diffraction (XRD), infrared (IR) spectroscopy, Raman spectroscopy and high resolution transmission electron microscopy (HRTEM). Their thermal conversion opens an access to Mn_3O_4 (hausmannite) and β-MnO_2 (pyrolusite) nanorods, respectively, under argon or air atmosphere. A coercive field of 12.4 kOe was obtained for the Mn_3O_4 nanorods.

Keywords: Manganese oxide; Nanorods; MnOOH; Manganite; MnO_2; Pyrolusite; Mn_3O_4; Hausmannite; Magnetic cluster; Thermal properties

1. Introduction

Nanorods and nanowires represent a class of one-dimensional nanostructures in which the carrier motion is restricted in two directions. Due to quantum confinement or surface effects, they usually show interesting properties that cannot be observed for their bulk counterparts of the same chemical composition [1,2]. In the recent years, these nanostructures have become the focus of intensive research activity owing to their applications in mesoscopic physics and fabrication of nanoscale electronic, optoelectronic and magnetic devices [3,4]. Manganese oxide and oxohydroxide one-dimensional nanostructures have attracted a great deal of attention because of their potential applications in many fields including separation, chemical sensing devices, biology and electronics. Among them, α- and γ-MnOOH, α-, β-and γ-MnO_2 present particular interest because of their applications as catalysts and as electrode materials in lithium batteries [5–12]; Mn_3O_4 possesses interesting magnetic [13,14], electrochemical properties [15–17] and may be used as an efficient catalyst for several processes [18–21]. The performance of manganese oxides in most of these applications could be potentially enhanced by processing one-dimensional nanostructures with well-controlled composition, dimensions and morphology. Chemical synthesis provides an interesting approach in terms of the best control of chemical composition, phase purity and material diversity [22]. A common chemical preparation of manganese

*Corresponding authors. Fax: +33 4 67 14 38 52.
E-mail addresses: joulia@univ-montp2.fr (J. Larionova), guari@univ-montp2.fr (Y. Guari).

0022-4596/$ - see front matter © 2005 Elsevier Inc. All rights reserved.
doi:10.1016/j.jssc.2005.05.018

oxide one-dimensional nanostructures consists in the hydrothermal synthesis in the presence of catalysts or template agents. Indeed, the preparation of α-MnOOH (groutite) elongated particles [5], γ-MnOOH (manganite) nanorods [6], α-MnO_2 nanorods [7,8], β-MnO_2 (pyrolusite) nanowires [9] and nanorods [10], γ-MnO_2 (ramsdellite) [8] and Mn_3O_4 [12] nanowires has been reported using $MnSO_4$, $Mn(CH_3COO)_2$, $KMnO_4$ salts or from commercial granular manganese oxides. An alternative strategy in the chemical preparation of metal oxide one-dimensional nanostructures consists in the use of molecular precursors [23,24]. However, this method has not been extended to the fabrication of manganese oxide nanostructures up to now. To the best of our knowledge, an unique example of using the coordination-polymer $[Mn(SO_4)(4,4'\text{-bpy})(H_2O)_2]_n$ as precursor in the preparation of γ-MnO_2 nanowires has been reported [25].

Herein, we report a novel cluster growth method for the synthesis of single-crystal γ-MnOOH nanorods by low-temperature hydrothermal treatment of $[Mn_{12}O_{12}(RCOO)_{16}(H_2O)_n]$ ($R = CH_3$ $(n = 4)$, C_2H_5 $(n = 3)$) without any catalysts or template agents. The thermal conversion of the so-obtained MnOOH nanorods provides an access to the fabrication of Mn_3O_4 (hausmannite) and β-MnO_2 (pyrolusite) nanorods.

2. Experimental section

2.1. Synthesis

All of the chemical reagents used in these experiments were analytical grade. The carboxylate clusters $[Mn_{12}O_{12}(CH_3COO)_{16}(H_2O)_4]\cdot 2CH_3COOH\cdot 4H_2O$ [26] (Fig. 1S, Supplemental Data), $[Mn_{12}O_{12}(C_2H_5COO)_{16}(H_2O)_3]\cdot 4H_2O$ [27], $[Mn_{12}O_{12}(C_6H_5COO)_{16}(H_2O)_4]\cdot C_6H_5COOH\cdot CH_2Cl_2$ [28] and $[Mn_{12}O_{12}(ClCH_2COO)_{16}(H_2O)_4]\cdot 6H_2O\cdot 2CH_2Cl_2$ [29] were prepared according to literature procedures.

2.1.1. Synthesis of γ-MnOOH nanorods 1

In a typical experiment, the cluster $[Mn_{12}O_{12}(CH_3COO)_{16}(H_2O)_4]\cdot 2CH_3COOH\cdot 4H_2O$ (0.1 g, 0.048 mmol) was dissolved in 25 mL of CH_3CN, filtered and added to 25 mL of an aqueous solution of NaOH (pH = 13.25). The mixture was vigorously stirred for 2 h. The resulting dark brown solution was transferred to a Teflon lined autoclave and heated at 150 °C for 24 h. The resulting brown solid was filtered, copiously washed with H_2O/CH_3CN (1/1), acetone, pentane and dried in vacuo at 80 °C for one night. Yield 0.048 g (95%).

For **1**, elemental analysis, calcd., %: Mn, 62.46; O, 36.41; found, % : Mn, 61.29; O, 36.26.

The clusters $[Mn_{12}O_{12}(C_2H_5COO)_{16}(H_2O)_3]\cdot 4H_2O$, $[Mn_{12}O_{12}(C_6H_5COO)_{16}(H_2O)_4]\cdot C_6H_5COOH\cdot CH_2Cl_2$ and $[Mn_{12}O_{12}(ClCH_2COO)_{16}(H_2O)_4]\cdot 6H_2O\cdot 2CH_2Cl_2$ were treated in the same experimental conditions in order to obtain the solids **1a**, **1b** and **1c**, respectively.

2.1.2. Preparation of Mn_3O_4 nanorods 2

Mn_3O_4 nanorods **2** were prepared by the calcinations of **1** up to 400 °C for 20 min under an argon flow with a heating rate of 2 °C min^{-1}.

For **2**, elemental analysis, calcd., %: Mn, 72.03; O, 27.97; found, %: Mn, 71.35; O, 29.32.

2.1.3. Preparation of β-MnO_2 nanorods 3

MnO_2 nanorods **3** were prepared by the calcinations of **1** up to 400 °C for 20 min under an air flow with a heating rate of 2 °C min^{-1}.

For **3**, elemental analysis, calcd., %: Mn, 63.19; O, 36.81; found, %: Mn, 63.40; O, 36.29.

2.2. Physical measurements

Thermogravimetric analyses (TGA/DTA) were performed on a NETZSCH STA 409 PC LUXX instrument. Infrared (IR) spectra were recorded on a Perkin Elmer 1600 spectrometer with a 4 cm^{-1} resolution. Elemental analyses were performed by the Service Central d'Analyse (CNRS, Vernaison, France). The samples were heated at 3000 °C under He. Oxygen was transformed in CO and detected by using an IR detector. Manganese was determined by using the emission spectroscopy technique PLASMA ICP. Powder X-ray diffraction (XRD) patterns were measured on a PanAnalytical diffractometer equipped with an ultra-fast X'celerator detector X'pert Pro in the 2Θ range (10–60)° with Nickel-filtered copper radiation (1.5405 Å). The measurement parameters are: stepsize, 0.01671; counting time, 60 s. Raman spectra were recorded with a laser spectrometer LABRAM 1B confocal of the Jobin–Yvon–Dilor–Spex Society. The emission of an helium-neon laser at wavenumber of 632.8 nm was used for measurements and a standard photon counting technique was used for detection. Magnetic susceptibility data were collected with a Quantum Design MPMS-XL SQUID magnetometer working in the temperature range of 1.8–300 K and the magnetic field range of 0–50 kOe. The data were corrected for the sample holder and the diamagnetism contributions calculated from the Pascal's constants [30]. Samples for high resolution transmission electron microscopy (HR TEM) measurements were prepared using ultramichrotomy techniques and then deposited on copper grids. HRTEM measurements were carried out at 200 kV with a microscope JEOL JEM 2010. Scanning electron microscopy (SEM) observations were performed at 15 kV on a JSM6300f. The solid sample was mounted on an adhesive support without any dispersion treatment. The nanorods size distribution

histograms were determined using enlarged SEM micrographs taken at magnification of $\times 25\,K$. A large number of nanorods (400–600) were counted in order to obtain a size distribution with good statistics.

3. Results

3.1. Synthesis of γ-MnOOH nanorods 1

The MnOOH nanorods **1** were prepared by hydrolysis of the cluster $[Mn_{12}O_{12}(CH_3COO)_{16}(H_2O)_4]\cdot 2CH_3COOH\cdot 4H_2O$ in CH_3CN for 24 h. The Mn/O ratio in **1** determined by elemental analysis is equal to 1.69 (expected value: 1.71). All of the reflections of the XRD pattern (Fig. 1a) were readily indexed to a pure monoclinic phase of γ-MnOOH (manganite, space group $P2_1/c$ (14)) with lattice parameters $a = 5.300\,Å$, $b = 5.278\,Å$, $c = 5.307\,Å$ and $\beta = 114{,}36^\circ$ (PDF 41-1379) [31]. In the 400–700 cm^{-1} range, the IR spectrum of sample **1** (Figure 2Sa, Supplemental Data) corresponds to the Mn–O stretching vibrations besides bands at 1089, 1120 and 1153 cm^{-1} characteristic of the OH-bending modes (respectively ν-OH, δ-2-OH and δ-1-OH) [32]. The broad bands at 2084 and 2672 cm^{-1} correspond to the fundamental O–H stretching bands related to hydrogen bonds, with an O–H.O length of about 2.6–2.7 Å in the structure of manganite [31]. The Raman spectrum of **1** presents peaks at 354, 385, 526, 554 and 620 cm^{-1} (Figure 3Sa, Supplemental Data) as observed in the spectrum of bulk MnOOH samples [33].

The panoramic morphology of the so-obtained product **1** was examined by SEM and HRTEM. The product **1** consists of nanorods, the proportion of which in the product is above 90% (Figs. 2a, b). Each nanorod is straight and has an uniform diameter along its entire length. Their average width is equal to 120 nm (Fig. 4S, Supplemental Data), while their length is about 1100 nm; the aspect ratio is around 9 [34]. Fig. 3a shows HRTEM image of a single MnOOH nanorod (aspect ratio 9.2) revealing its monocrystalline structure. It is structurally uniform with a periodic fringe spacing of 3.57 Å along the longitudinal axis of the nanorod, which corresponds to the interplanar spacing between the (011) planes of the monoclinic MnOOH. Thus, the longitudinal axis of the MnOOH nanorods corresponds to the *b* axis of the monoclinic cell unit. The electron diffraction pattern of a single MnOOH nanorod obtained by focusing the electron beam perpendicular to the longitudinal axis is presented in Fig. 3b.

The following clusters were treated under the same experimental conditions as for **1**: $[Mn_{12}O_{12}(C_2H_5COO)_{16}(H_2O)_3]\cdot 4H_2O$, $[Mn_{12}O_{12}(C_6H_5COO)_{16}(H_2O)_4]\cdot C_6H_5COOH\cdot CH_2Cl_2$ and $[Mn_{12}O_{12}(ClCH_2COO)_{16}(H_2O)_4]\cdot 6H_2O\cdot 2CH_2Cl_2$. Brown solids respectively named **1a**, **1b**, and **1c** were obtained. In all cases, the formation of the manganite phase, γ-MnOOH, was observed. SEM measurements indicate that nanorods in proportion of about 90% were formed only in the case of **1a** (Figure 5Sa, b, Supplemental Data). The SEM images of **1b** and **1c** show melted nanorods in which the proportion of nanorods is only around 40–50% (Figure 5Sc, d, Supplemental Data).

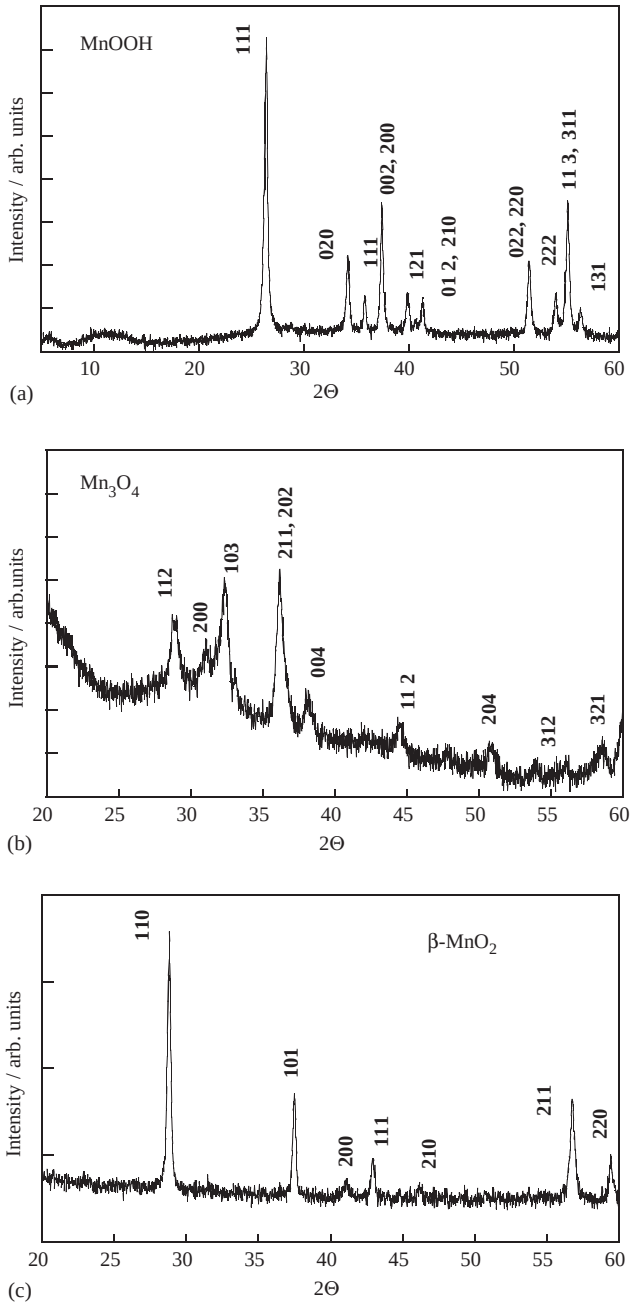

Fig. 1. Powder X-ray diffraction pattern within the range 2θ (5–60°) for : (a) **1**; (b) the sample **1** heated under argon at 400 °C; (c) the sample **1** heated at 400 °C under air.

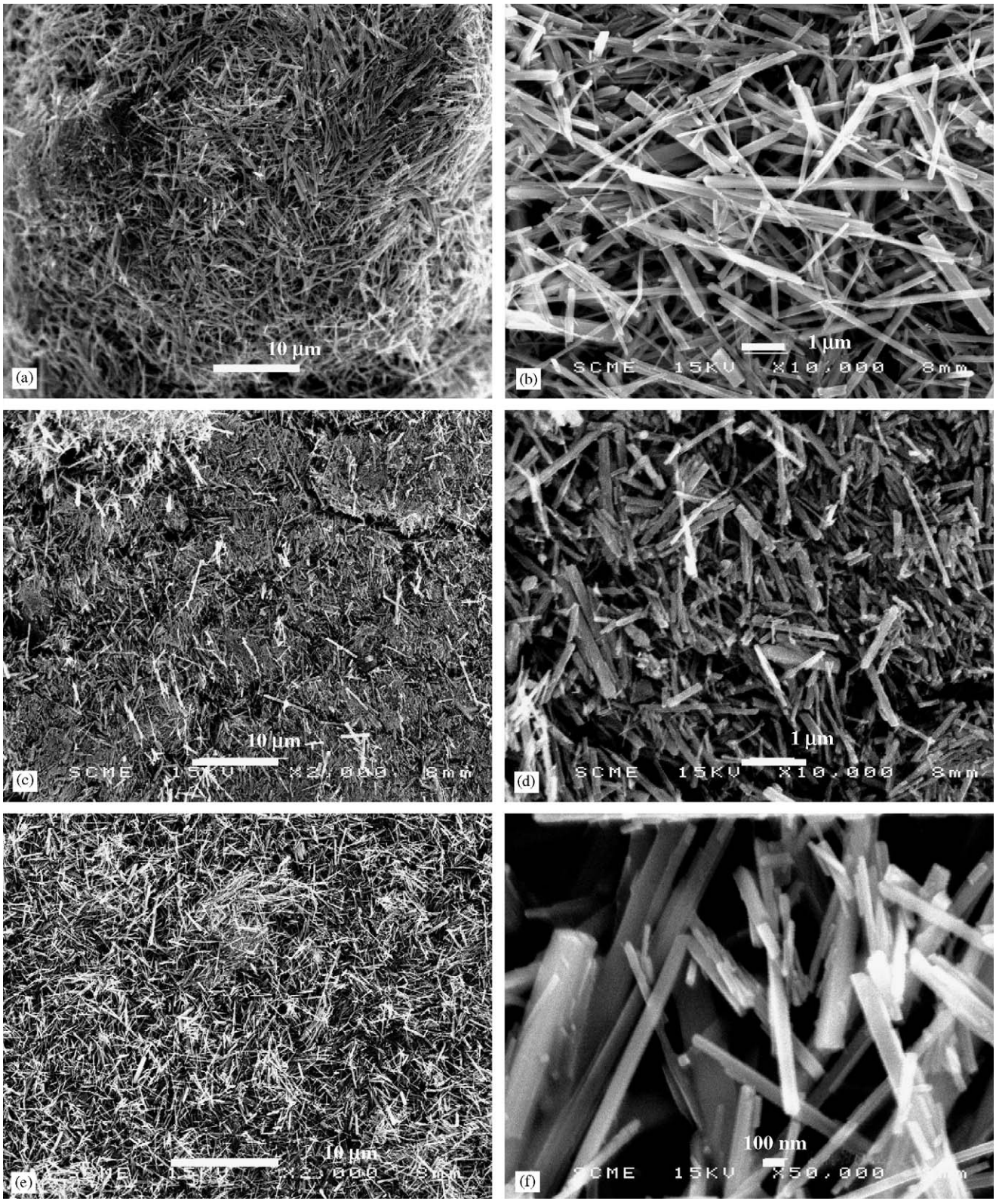

Fig. 2. Scanning electron microscopy (SEM) image of (a), (b) MnOOH nanorods **1**; (c), (d) Mn_3O_4 nanorods **2** and (e), (f) β-MnO_2 nanorods **3**.

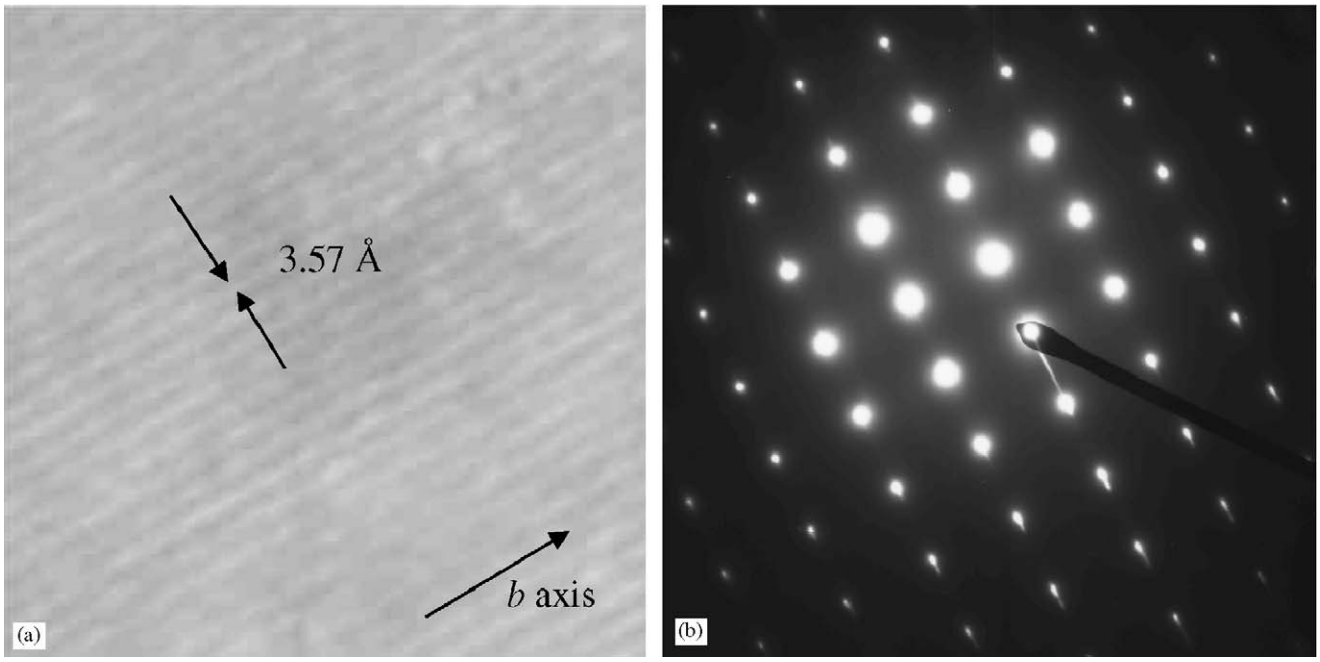

Fig. 3. High resolution transmission electron microscopy (HRTEM) image (a) of a single MnOOH nanorod of **1** and (b) electron diffraction pattern of the same MnOOH nanorod.

3.2. Formation of Mn_3O_4 nanorods: the thermal behaviour of the MnOOH nanorods *1* under argon atmosphere

The thermogravimetric analysis (TGA-DTA) of **1** performed under argon atmosphere from room temperature up to 1200 °C exhibits three well-pronounced weight loss steps with inflexion points at 272, 522, and 1060 °C which correspond to weight losses of 12.9%, 1.7% and 0.6%, respectively (Fig. 4a).

The first weight loss (inflexion point at 272 °C) of 12.9% (expected value: 13%) is assigned to the transformation of MnOOH into Mn_3O_4 and oxygen and water release according to Eq. (1):

$$6MnOOH \rightarrow 2Mn_3O_4 + 3H_2O + \tfrac{1}{2}O_2. \quad (1)$$

The XRD pattern of sample **2** obtained by heating sample **1** up to 400 °C under argon is shown in Fig. 1b. All diffraction peaks can be indexed to the pure tetragonal phase (space group: $I41/amd$) of Mn_3O_4 (hausmannite) with lattice parameters $a = 5.76$ Å and $c = 9.47$ Å (PDF 24-0734). IR bands observed at 603, 492 and 419 cm^{-1} (Figure 2Sb, Supplemental Data) along with a strong peak at 642 cm^{-1} in the Raman spectrum of this solid (Figure 3Sb, Supplemental Data) are characteristic of Mn_3O_4 [35–38].

The SEM measurements depicted in Figs. 2c, d show that sample **2** consists of nanorods with a proportion in the product above 90% with an aspect ratio around 7 (Fig. 6S, Supplemental Data).

A temperature dependence of the magnetization for **2** performed with an applied magnetic field of 100 Oe is shown in Fig. 5a. The curve increases dramatically below 60 K with an inflexion point at 42 K indicating the critical temperature for this compound. This value corresponds to the critical temperature previously observed for bulk Mn_3O_4 [39,40] or nanoparticles with sizes larger than 10 nm [41,42]. The in-phase (χ'_M) and the out-of-phase (χ''_M) components of alternating current (ac) susceptibility performed at three different frequencies 1, 49 and 1000 Hz in zero applied direct current (dc) field also show peaks at 42 K. No frequency-dependent behaviour characteristic of superparamagnetic behaviour of nanoparticles (size < 10 nm) [41] can be observed (Fig. 7S, Supplemental Data).

The field dependence of the magnetization for **2** is clearly consistent with a nanorod structure. The calculated value of the saturation magnetization (16755 emu mol^{-1}) is not reached at 50 kOe. A hysteresis behaviour with a coercive field of 12.4 kOe was observed as the magnetic field was varied from 50 kOe to –50 kOe (Fig. 5b).

3.3. Formation of β-MnO_2 nanorods: the thermal behaviour of the MnOOH nanorods *1* under air

The thermogravimetric analysis of the product **1** performed under air from room temperature up to 1200 °C exhibits three well-pronounced weight loss steps at 250, 556 and 943 °C (Fig. 4b).

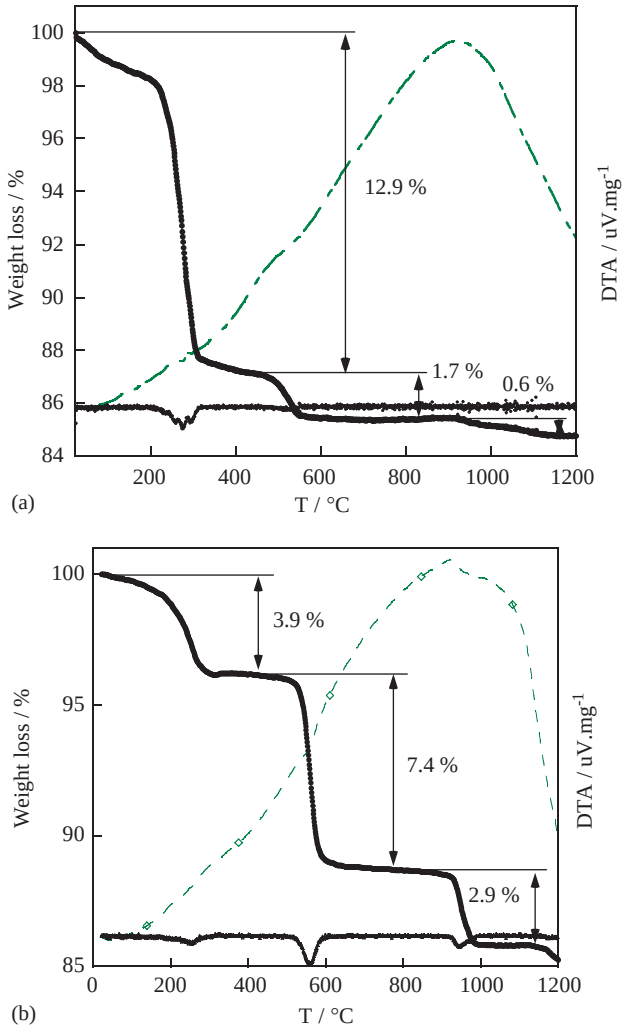

Fig. 4. Thermogravimetric analysis (TGA) weight loss, wt% (-♦-) and DTA curve (---) of MnOOH nanorods **1** (a) performed under argon atmosphere and (b) performed under air.

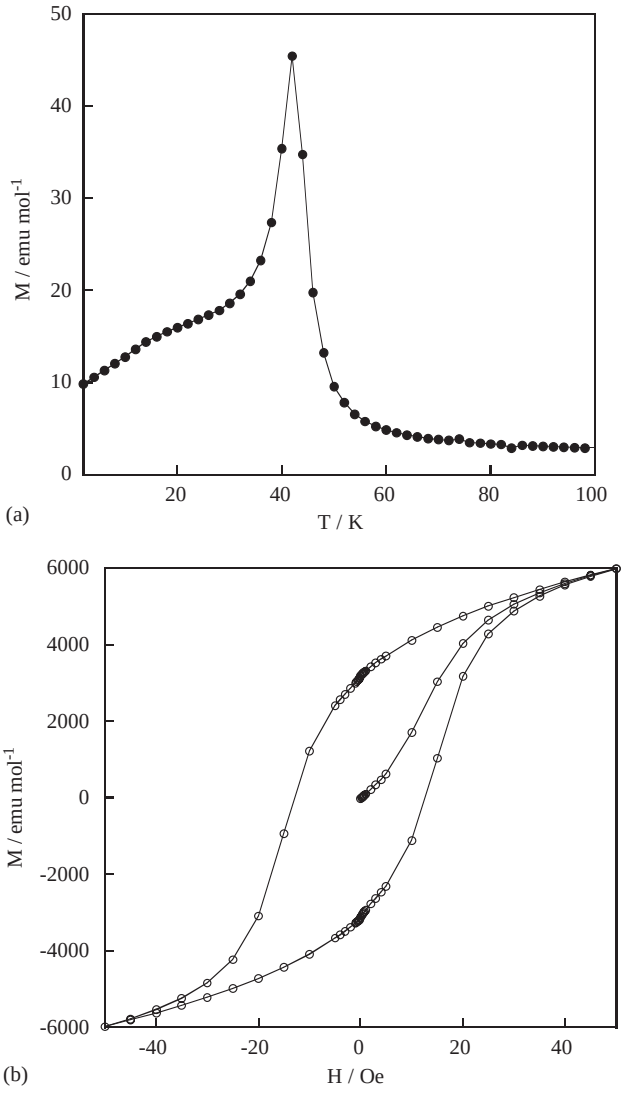

Fig. 5. (a) Temperature dependence of the magnetization performed with an applied magnetic field of 100 Oe for sample **2**; (b) field dependence of the magnetization for **2** showing hysteresis behaviour.

The first weight loss (inflexion point at 250 °C) of 3.9% (expected value: 1.1%) corresponds to the oxidation of γ-MnOOH (manganite) phase into β-MnO_2 (pyrolusite) according to the reaction (2) and to the oxidation of residual organic moieties:

$$4MnOOH + O_2 = 4MnO_2 + 2H_2O. \quad (2)$$

The XRD pattern of sample **3** (Fig. 1c) obtained by heating sample **1** up to 400 °C under air presents peaks consistent with a pure tetragonal phase (space group: P42/mnm (136)) of β-MnO_2 (pyrolusite) with lattice parameters $a = 4.38$ Å and $c = 2.86$ Å (PDF 72-1984). Its IR spectrum displays bands at 411, 527 and 712 cm^{-1} due to the Mn–O vibrations (Figure 2Sc, Supplemental Data) [33]. In addition, its Raman spectrum exhibits a strong peak at 655 cm^{-1} characteristic of β-MnO_2 (Figure 3Sc, Supplemental Data) [43].

The SEM images of **3** shown in Figs. 2e, f reveal that the morphology of the nanorods was completely preserved upon heating at 400 °C under air. The aspect ratio of the nanorods **3** is equal to 7 (Fig. 11S, Supplemental Data).

The second and third weight loss steps of 7.4% and 2.9%, respectively, with inflexion points at 556 and 943 °C (Fig. 4b) correspond to oxygen release and the transformation of β-MnO_2 (pyrolusite) to Mn_2O_3 (bixbyite) according to Eq. (3) and the subsequent conversion of Mn_2O_3 to Mn_3O_4 according to Eq. (4):

$$6MnO_2 = 3Mn_2O_3 + \tfrac{3}{2}O_2, \quad (3)$$

$$3Mn_2O_3 = 2Mn_3O_4 + \tfrac{1}{2}O_2. \quad (4)$$

SEM images performed on these samples show a destruction of the initial nanorods **1** (see Supplemental Data for XRD, spectroscopic characterisations and SEM).

4. Discussion

A novel cluster growth method has been developed to synthesize γ-MnOOH (manganite) nanorods by low-temperature hydrothermal treatment of the clusters $[Mn_{12}O_{12}(RCOO)_{16}(H_2O)_n]$ ($R = CH_3$ ($n = 4$), C_2H_5 ($n = 3$)) without any catalyst or template. The use of $[Mn_{12}O_{12}(RCOO)_{16}(H_2O)_n]$ ($R = CH_3$, CH_2Cl, C_6H_5 ($n = 4$) and C_2H_5 ($n = 3$)) species as molecular precursors in the synthesis of manganese oxohydroxide nanorods was appealing for the following reasons:

(i) $[Mn_{12}O_{12}(RCOO)_{16}(H_2O)_n]$ have a pre-formed oxo-manganese core containing a central $[Mn^{IV}_4O_4]$ cuban surrounded by a nonplanar ring of eight outer Mn^{III} ions that are bridged and connected to the cube via μ_3-O^{2-} ions (see Supplemental Data) [26–29];
(ii) The clusters may be easily hydrolysed in the presence of water and their thermal treatment give rise to pure bulk manganese oxides [41]. The thermal treatment may be performed under different atmospheres.
(iii) The peripheral ligation of the clusters is performed by 16 bridging labile carboxylate ligands, which may be easily removed and exchanged with a large range of carboxylate groups $RCOO^-$ without change of the oxo-manganese cluster core. The lability of the peripheral ligands is influenced by the nature of R.

A first point to note concerns the phase purity, homogeneity and the narrow size distribution of the so-obtained nanorods. To the best of our knowledge, the sole previously published synthesis of γ-MnOOH has been performed by using $KMnO_4$ as precursor and ethanol as reducing agent [6]. Nanorods with a large diameter distribution between 50 and 500 nm with lengths of tens of micrometers were obtained. In this method, the influence of the amount of ethanol in the solvent along with the reaction temperature on both the morphology and the composition of the final product were shown to be very important. As a consequence, other phases, such as K_xMnO_2 or Mn_3O_4, may be obtained beside MnOOH. In contrast, the use of $[Mn_{12}O_{12}(RCOO)_{16}(H_2O)_n]$ as precursor does not required the employment of strict reaction conditions and no impurities were detected on the final nanorods. The so-obtained γ-MnOOH nanorods posses a narrow diameter distribution centred at 120 nm along their entire length and an aspect ratio around 9.

A clear morphology dependence of the MnOOH nanorods on the nature of the peripheral ligation of the $[Mn_{12}O_{12}(RCOO)_{16}(H_2O)_n]$ cluster precursor was established. Well-formed nanorods were obtained when using manganese clusters bearing carboxylate ligands $RCOO^-$ with $R = CH_3$ and C_2H_5, while melted nanorods in which the proportion of nanorods is less than 50% were obtained for $R = ClCH_2$ and C_6H_5. These results strongly suggest that the carboxylate ligands play the role of structuring agent in the synthesis and that the increase of the electron donating capacity of the R groups favours the nanorods formation.

Another point to note concerns the transformation of γ-MnOOH nanorods into Mn_3O_4 and β-MnO_2. For the bulk solids, the manganite–pyrolusite (MnOOH $\rightarrow$ β-MnO_2) conversion upon heating under air is known in the literature and takes place at 350 ° [31]. However, no investigations have been reported on the manganite transformations upon heating under different atmospheres at the nano-sized level. The thermal conversion of the so-obtained MnOOH nanorods performed both under argon and air atmospheres provides an access to the formation of Mn_3O_4 (hausmannite) and β-MnO_2 (pyrolusite) nanorods. In comparison to bulk materials, the lower conversion temperatures of 275 °C (for Mn_3O_4) and 250 °C (for β-MnO_2) can be attributed to the higher surface of the nanorods. In both cases, the initial nanorods morphology was preserved after thermal treatment with a slight modification of the aspect ratio from 9 to 7. It is noteworthy that the coercive field observed for the obtained Mn_3O_4 nanorods is much larger than the ones reported previously for bulk Mn_3O_4 (3 kOe) [39,40], aggregated Mn_3O_4 nanoparticles (6.1 kOe) [44] or Mn_3O_4 nanoparticles of around 10 nm (2.5 kOe) [41]. Obviously, the large H_c value has been achieved by two main factors: the shape anisotropy due to the nanorods morphology [45] and the formation of a single magnetic domain due to the small nanorods size [46].

Acknowledgments

The authors thank Dr. Arie van der Lee (IEM, UMR 5635, Montpellier, France) for XRD measurements and for helpful discussions, Mr. L. Datas (TEMSCAN, Toulouse, France) for HRTEM measurements, Service Central d'Analyse (CNRS, Vernaison, France). The authors thank the CNRS and the Université Montpellier II for financial support.

Appendix A. Supplemental Data

The online version of this article contains additional supplementary data. Please visit doi:10.1016/j.jssc.2005.05.018.

References

[1] W.U. Huynh, J.J. Dittmer, A.P. Alivisatos, Science 295 (2002) 2425–2427.
[2] X. Duan, Y. Huang, Y. Gui, J. Wang, C.M. Lieber, Nature 409 (2001) 66–72.
[3] Z.L. Wang, Adv. Mater. 12 (2000) 1295–1298.
[4] Y. Xia, P. Yang, Y. Sun, Y. Wu, B. Mayers, B. Gates, Y. Yin, F. Kim, H. Yan, Adv. Mater. 15 (2003) 353–389.
[5] M. Ocana, Colloid Polym. Sci. 278 (2000) 443–449.
[6] W. Zhang, Z. Yang, Y. Liu, S. Tang, X. Han, M. Chen, J. Cryst. Growth 263 (2004) 394–399.
[7] X. Wang, Y. Li, Chem. Commun. (2002) 764–765.
[8] N. Kijima, H. Yasuda, T. Sato, Y. Yoshimura, J. Solid State Chem. 159 (2001) 94–102.
[9] X. Wang, Y. Li, J. Am. Chem. Soc. 124 (2002) 2881–2882.
[10] G. Xi, Y. Peng, Y. Zhu, L. Xu, W. Zhang, W. Yu, Y. Qian, Mater. Res. Bull. 39 (2004) 1641–1648.
[11] Z.-Y. Yuan, Z. Zhang, G. Du, T.-Z. Ren, B.-L. Su, Chem. Phys. Lett. 378 (2003) 83–86.
[12] W. Wang, C. Xu, G. Wang, Y. Liu, C. Zheng, Adv. Mater. (2002) 837–840.
[13] Y. Yafet, C. Kittel, Phys. Rev. 87 (1952) 290–294.
[14] A.R. Armstrong, P.G. Bruce, Nature 381 (1996) 499–500.
[15] Y.F. Shen, R.P. Zerger, R.N. Deguzman, S.L. Suib, L. McCurdy, D.I. Potter, C.L. O'Young, Science 260 (1993) 511–515.
[16] Q. Feng, H. Karoh, K. Ooi, M. Tani, Y.J. Nakacho, J. Electrochem. Soc. 141 (1994) L135.
[17] S.C.D. Torresi, A. Gorenstein, Electrochim. Acta 37 (1992) 2015–2019.
[18] E.R. Stobhe, B.A. Boer, J.W. Geus, Catal. Today 47 (1999) 161–167.
[19] E. Grootendorst, Y. Verbeek, V. Ponec, J. Catal. 157 (1995) 706–712.
[20] M. Baldi, E. Finocchio, F. Milella, G. Busca, Appl. Catal. B, Environ. 16 (1998) 43–51.
[21] M.F.M. Zwinkels, S.G. Jaras, P.G. Menon, T.A. Griffik, Catal. Rev. Sci. Eng. 35 (1993) 319–358.
[22] Y. Xia, J.A. Rogers, K.E. Paul, G.M. Whitesides, Chem. Rev. 99 (1999) 1823–1848.
[23] P. Yan, Y. Xie, Y. Qian, X. Liu, Chem. Commun. (1999) 1293–1294.
[24] K. Soulantica, A. Maisonnat, F. Senocq, M.-C. Fromen, M.-J. Casanove, B. Chaudret, Angew. Chem. Int. Ed. 40 (2001) 2983–2986.
[25] Y. Xiong, Y. Xie, Z. Li, C. Wu, Chem. Eur. J. 9 (2003) 1645–1651.
[26] T. Lis, Acta Cryst. B 36 (1980) 2042–2046.
[27] H.J. Eppley, H.-L. Tsai, N. de Vries, K. Folting, G. Christou, D.N. Hendrickson, J. Am. Chem. Soc. 117 (1995) 301–317.
[28] R. Sessoli, H.L. Tsai, A.R. Schake, S. Wang, J.B. Vincent, K. Folting, D. Gatteschi, G. Christou, D.N. Hendrickson, J. Am. Chem. Soc. 115 (1993) 1804–1816.
[29] J. An, Z.-D. Chen, X.-X. Zhang, H.G. Raubenheimer, C. Esterhuysen, S. Gao, G.X. Xu, J. Chem. Soc., Dalton Trans. (2001) 3352–3356.
[30] E.A.L. Boudreaux, N. Mulay, Theory and Applications of Molecular Paramagnetism, Wiley, New York, 1976.
[31] T. Kohler, T. Armbrustor, E. Libowitzky, J. Solid State Chem. 133 (1997) 486–500.
[32] A. Novak, Struct. Bond. 18 (1974) 177–216.
[33] C.M. Julien, M. Massot, C. Poinsignon, Spectrochim. Acta A 60 (2004) 689–700.
[34] J. Murphy, N.R. Jana, Adv. Mater. 14 (2002) 80–82.
[35] W. Zhang, Z. Yang, Y. Liu, Sh. Tang, X. Han, M. Chen, J. Cryst. Growth 263 (2004) 394–399.
[36] B. Gillot, M. El Guendouzi, M. Laarj, Mater. Chem. Phys. 70 (2001) 54–60.
[37] M.C. Bernard, A.H.L. Goff, B.V. Thi, J. Electrochem. Soc. 140 (1993) 3065.
[38] Y. Lui, Z. Lui, G. Wang, Appl. Phys. A 76 (2003) 1117–1120.
[39] G. Srinivasan, M.S. Seehra, Phys. Rev. B 28 (1983) 1–7.
[40] K. Dwight, N. Menyuk, Phys. Rev. 119 (1960) 1470–1479.
[41] B. Folch, J. Larionova, Y. Guari, Ch. Guérin, A. Mehdi, C. Reye, J. Mater. Chem. 14 (2004) 2703–2711.
[42] W.S. Seo, H.H. Jo, K. Lee, B. Kim, S.J. Oh, J.T. Park, Angew. Chem. Int. Ed. 43 (2004) 1115–1117.
[43] C. Julien, M. Massot, S. Rangan, M. Lemal, D. Guyomard, J. Raman Spectrosc. 33 (2002) 223–228.
[44] A. Buckelew, J.R. Galan-Mascaros, K. Dunbar, Adv. Mater. 14 (2002) 1646–1648.
[45] A. Herpin, Théorie du magnétisme, Ed. PUF, Paris, 1968, p. 37.
[46] J. Jin, S.-I. Okhoshi, K. Hashimoto, Adv. Mater. 16 (2004) 48–51.